Biochimica et Biophysica Acta 1808 (2011) 2466–2476

Contents lists available at ScienceDirect

Biochimica et Biophysica Acta

journal homepage: www.elsevier.com/locate/bbamem

Glycolipid–cholesterol monolayers: Towards a better understanding of the interaction between the membrane components

Beata Korchowiec [a,*], Jacek Korchowiec [b], Masakatsu Hato [c,d], Ewa Rogalska [e,*]

[a] Department of Physical Chemistry and Electrochemistry, Faculty of Chemistry, Jagiellonian University, ul. R. Ingardena 3, 30-060 Krakow, Poland
[b] Department of Theoretical Chemistry, Faculty of Chemistry, Jagiellonian University, ul. R. Ingardena 3, 30-060 Krakow, Poland
[c] RIKEN Systems and Structural Biology Center, 1-7-22 Suehiro-cho, Tsurumi-ku, Yokohama, Kanagawa-230-0045, Japan
[d] Nanotechnology Research Institute, AIST. Tsukuba Central-5, Higashi 1-1-1, Tsukuba, Ibaraki 305-8565, Japan
[e] Equipe GEVSM, Structure et Réactivité des Systèmes Moléculaires Complexes, UMR 7565 Nancy Université/CNRS, BP 239, 54506 Vandoeuvre-lès-Nancy cedex, France

ARTICLE INFO

Article history:
Received 15 April 2011
Received in revised form 29 June 2011
Accepted 30 June 2011
Available online 14 July 2011

Keywords:
Model biological membranes
Binary mixture
Langmuir monolayers
Lipid miscibility
Molecular dynamics simulation

ABSTRACT

In this work, the interaction between a synthetic analog of archaeal lipids and cholesterol was studied using Langmuir technique. The lipid, β-$Mal_3O(C_{16+4})_2$, contained phytanyl chains attached via two ether bonds to the *sn*-2 carbon of the glycerol backbone. The preliminary studies showed that monolayers formed with the pure lipid have a liquid-like character; here, a hypothesis that admixing cholesterol to β-$Mal_3O(C_{16+4})_2$ could confer a higher rigidity on the films was tested.

To check this proposal, two-dimensional miscibility of cholesterol and β-$Mal_3O(C_{16+4})_2$ in monomolecular films was studied using surface pressure and surface potential measurements, as well as Brewster angle microscopy and polarization-modulation infrared reflection absorption spectroscopy. The stability of the monomolecular films was evaluated based on thermodynamics of mixing of cholesterol and β-$Mal_3O(C_{16+4})_2$. Atomic level information concerning the orientation of molecules and the degree of hydration of polar headgroups was obtained from molecular dynamics simulations.

1. Introduction

Since 1962, when a diether-linked lipid from *Halobacterium cutrirubrum* was first described, over 100 ether-based phospho-, glyco- and phosphoglycolipids have been identified in various archaea [1]. The diether lipids are found in almost all archaea, whereas the tetraether structures, termed caldarchaeols and calditoglycerocaldarchaeols, are found only in methanogenic, thermophilic and psychrophilic archaea [2]. Archaeal lipids [3,4] and their analogs are interesting for different applications, [5–8] such as novel delivery systems of drugs and vaccines, matrices for reconstitution of labile membrane proteins, and for crystallization of membrane proteins [9]. Polar glycerolipids make up the bulk of the archaebacteria membrane lipids, with the remaining neutral lipids being primarily squalenes and other hydrocarbons [10]. The polar lipids contain regularly branched, and usually fully saturated 3,7,11,15-tetramethylhexadecyl (phytanyl) chains [11,12] of 20, 25, or 40 carbon length, with the 20 and 40 being most common. The phytanyl chains are attached via ether bonds to the *sn*-2 and *sn*-3 carbons of the glycerol backbone. The highly branched hydrophobic groups of these lipids are different from those of other organisms. Indeed, most membrane lipids bear two linear hydrocarbon chains of variable length and degree of unsaturation, ester-linked to a glycerol group which third hydroxyl is linked to a polar residue. It is supposed that the phytanyl-based lipids play important physiological roles in maintaining membrane functions under harsh environmental conditions [11–13]. The higher chemical stability, conformational rigidity and pressure tolerance make archaeal ether lipid membranes better suited to extreme environments than the ester-linked lipids found in bacterial or eukaryal membranes [14].

It has been shown recently that polar archaebacterial lipids form liposomes. In general, archaea liposomes (archaeosome) demonstrate relatively higher stabilities to oxidative stress, high temperature, alkaline pH, action of phospholipases, bile salts, and serum proteins compared to their phosphoglyceride counterparts [7]. On the other hand, the fact that the human body is constantly exposed to archaeal-like lipids suggests that archaeosomes can be used as safe pharmaceutical adjuvants suitable for humans [6].

Because extraction and fractionation of archaeal lipids from cell membranes in large amounts are difficult, chemically pure archaeal lipid analogs are often synthesized [8]. A new class of stereochemically pure nonionic phytanyl-chained glycolipids has been prepared as model archaeal diether lipids, namely 1,3-di-*O*-phytanyl-2-*O*-(β-glycosyl)-glycerols bearing maltooligosaccharide headgroups, β-$Mal_NO(C_{p+q})_2$, where N represents the number of glucose residues

* Corresponding authors.
E-mail addresses: bkorch@chemia.uj.edu.pl (B. Korchowiec), ewa.rogalska@srsmc.uhp-nancy.fr (E. Rogalska).

0005-2736/$ – see front matter © 2011 Elsevier B.V. All rights reserved.
doi:10.1016/j.bbamem.2011.06.027

in the headgroup, p is number of carbon atoms in the main chain and q is number of methyl groups, respectively; consequently, the 3, 7, 11, 15-tetramethylhexadecyl (phytanyl) group is denoted as C_{16+4} [14–16]. It can be expected that in physiological conditions the 1,3-ether derivatives would be less susceptible to undergo degradation compared to the natural 1,2-ethers. A sugar headgroup was chosen rather than phosphocholine one, because sugars are known to stabilize the native structure of proteins [17].

The fluidity of lipid membranes based on diether structures can be readily controlled through the number of phytanyl chains (1 or 2) ether-linked to the glycerol unit, the macrocyclization of the lipid chains and the presence of glycosidic polar heads. In particular, the glycolipids form strong intermolecular hydrogen bonds, resulting in a decrease of the lateral mobility of the molecules and, consequently, in a lower fluidity of the membranes [5]. On the other hand, the properties of lipid matrices can be fine tuned by admixing various components. The preliminary studies showed that the β-$Mal_3O(C_{16+4})_2$ monolayers have a liquid-like character [18]. It was observed previously that cholesterol increases the orientational order of the phospholipid hydrocarbon chains and induces a condensing effect in mixed phospholipid/CHOL [19,20] and glycolipid/CHOL [21] monolayers at the air/water interface. Here, a hypothesis that admixing cholesterol to β-$Mal_3O(C_{16+4})_2$ could confer a higher rigidity on the films was tested.

A better knowledge of the interaction between the archaea-like lipids and cholesterol may be useful for preparing mixed lipid systems with controlled microstructure for defined applications. Adjusting fluidity and permeability of liposomes and other types of bilayers may be important in drug delivery systems. Compared to lipid membranes in the form of bilayers, lipid monomolecular films (Langmuir films) are readily amenable to study via a rich variety of experimental techniques. Here, the two-dimensional miscibility of cholesterol and β-$Mal_3O(C_{16+4})_2$ in monomolecular films was studied using surface pressure and surface potential measurements, as well as Brewster angle microscopy (BAM) and PM-IRRAS. The results obtained are discussed in the light of a nonideal behavior of the mixtures. The stability of the monomolecular films was evaluated based on thermodynamics of mixing of cholesterol and β-$Mal_3O(C_{16+4})_2$. Atomic level information concerning the orientation of molecules and the degree of hydration of polar headgroups was obtained from molecular dynamics simulations.

2. Materials and methods

2.1. Materials and reagents

The synthesis and characterization of 1,3-di-*O*-phytanyl-2-*O*-(β-D-maltotriosyl)-glycerol, β-$Mal_3O(C_{16+4})_2$, were described previously [14]. The purity of β-$Mal_3O(C_{16+4})_2$ estimated by NMR and TLC was above 96%. Synthetic cholesterol (CHOL) (~99% pure) and chloroform (99.9% pure) were from Sigma-Aldrich. β-$Mal_3O(C_{16+4})_2$ and CHOL were dissolved in chloroform to achieve a final concentration of 0.5 mg mL^{-1}. The stock solutions of β-$Mal_3O(C_{16+4})_2$ and CHOL were used for preparing 0.2, 0.4, 0.5, 0.6, and 0.8 β-$Mal_3O(C_{16+4})_2$/CHOL mol fraction mixtures. The lipid solutions were stored at 4 °C. The distilled water was purified with a Millipore Milli-Q system, yielding a resistance of 18 MΩ cm and surface tension of 72.8 mN m^{-1} at 20 °C.

2.2. Compression isotherms and Brewster angle microscopy

The surface pressure–area (Π-*A*) isotherms were carried out with a KSV 2000 Langmuir balance (KSV Instruments, Helsinki). The isotherms were measured for pure lipid monolayers, as well as their various mixtures. The surface pressure was monitored using a platinum Wilhelmy plate. Surface potential (Δ*V*) was measured with a KSV Spot 1 (KSV Instruments, Helsinki) using a vibrating plate and a stainless steel counter electrode. The thermostated Teflon® trough of the effective film area of 765 cm^2 was equipped with two hydrophilic Delrin® barriers (symmetric compression). Before each measurement, the subphase surface was cleaned by sweeping and suction. The stability of the surface potential signal was checked before each experiment, after cleaning the water subphase. After the Δ*V* signal had reached the constant value it was zeroed, and the film was spread on the subphase. The lipid solutions were spread with a Hamilton syringe on the free surface of water and left for 15 min to allow solvent evaporation and to reach an equilibrium state of the monolayer. All isotherms were recorded upon symmetric compression of the monolayer at a constant barrier speed of 2.5 $Å^2$ $molecule^{-1}$ min^{-1}. In the case of binary mixtures, the surface pressure was plotted against the mean molecular area, obtained by dividing the total surface area by the number of lipid molecules spread on the surface. For each monolayer composition, measurements were repeated at least 3 times. The Π-*A* and Δ*V*-*A* isotherms were recorded at 20 ± 0.1 °C. The standard deviation obtained from compression isotherms was ± 0.5 $Å^2$ on molecular area (*A*), ± 0.2 mN m^{-1} on surface pressure and ± 0.01 V on surface potential.

The compression isotherms allowed determining the compressibility modulus, C_S^{-1}, [22] as:

$$C_S^{-1} = -A(\partial\Pi/\partial A)_T. \quad (1)$$

The collapse parameters, ΔV_{coll}, Π_{coll} and A_{coll}, corresponding to the highest packing of molecules in the monolayer were determined from the maximum of C_S^{-1} value. The excess free enthalpy of mixing, ΔG^{ex}, [23,24] was calculated from Π-*A* isotherms using the following formula:

$$\Delta G^{ex} = \int_0^{\Pi} [A_{12} - (X_1A_1 + X_2A_2)]d\Pi \quad (2)$$

where A_{12} is the mean molecular area in the mixed monolayer at a given surface pressure, A_1 and A_2 are the mean molecular areas of the pure components 1 and 2 at the same surface pressure, and X_1 and X_2 are the mole fractions of the two lipid components in the mixed film.

The morphology of the films was imaged with a computer-interfaced KSV 2000 Langmuir balance combined with a Brewster angle microscope (KSV Optrel BAM 300, Helsinki). The Teflon® trough dimensions were 6.5 cm × 58 cm × 1 cm; other experimental conditions were as described above.

2.3. Polarization-modulation infrared reflection-absorption spectroscopy

The PM-IRRAS spectra of β-$Mal_3O(C_{16+4})_2$, CHOL and mixed β-$Mal_3O(C_{16+4})_2$/CHOL monolayers of 0.2 and 0.8 mol fraction of CHOL spread on pure water subphase were registered at 20 °C. The Teflon® trough dimensions were 36.5 cm × 7.5 cm × 0.5 cm; other experimental conditions were as described in the preceding paragraph. The PM-IRRAS measurements were performed using a KSV PMI 550 instrument (KSV Instruments Ltd, Helsinki, Finland). The PMI 550 contains a compact Fourier Transform IR-spectrometer equipped with a polarization-modulation (PM) unit on one arm of a goniometer, and a MCT-detector on the other arm. The incident angle of the light beam can be freely chosen between 40°–90°; here, the incident angle was 79°. The spectrometer and the PM-unit operate at different frequencies, allowing separation of the two signals at the detector. The PM unit consists of a photoelastic modulator, which is an IR-transparent, ZnSe piezoelectric lens. The incoming light is continuously modulated between s- and p-polarization at a frequency of 74 kHz. This allows simultaneous measurement of spectra for the two polarizations, the difference providing surface specific information, and the sum providing the reference spectrum. As the spectra are measured simultaneously, the effect of water vapor is largely reduced. In the

mid-IR region, the wavenumber at which the half-wave retardation takes place can be freely selected. Here, the maximum of PEM efficiency was set either to 1500 or to 2900 cm^{-1} for analyzing the different regions of the spectra. The spectral range of the device is 800–4000 cm^{-1} and the resolution is 8 cm^{-1}.

2.4. Computational details

The simulation setup included a water slab bounded by two vacuum slabs. Two symmetric monolayers, each composed of 100 molecules, were placed at the vacuum/water interfaces. Pure CHOL and β-$Mal_3O(C_{16+4})_2$ monolayers, as well as, mixed β-$Mal_3O(C_{16+4})_2$/CHOL monolayers were investigated. 0.2 or 0.8 CHOL mole fraction, the same at both interfaces, was considered. Molecular dynamics (MD) calculations were carried out using NAMD2 package [25] and CHARM27 force field [26] including a rigid TIP3 water molecule [27]. The simulation was performed under constant number of particles (N), constant temperature (T), constant normal pressure (p_N), and constant surface tension (γ): $Np_N\gamma T$ ensemble [28]. Three dimensional boundary conditions were used. Depending on the system, the length of the simulation box normal to the monolayer (z-axis) was changed from 200 to 310 Å. Such length in this direction guaranteed that the interaction between periodic replicas was negligible. Accordingly, the thickness of the water slab changed from 50 to 90 Å. This variation was connected with the size of the hydrophilic part of β-$Mal_3O(C_{16+4})_2$. It was demonstrated that the presence of at least 20 Å thick slab of water guarantees the independence of two monolayers, [29] therefore, the water slab used in the current study should simulate the condition of monolayer experiment. The adequacy of the assumed symmetric model for describing monolayer film at water/air interface was confirmed by many research groups [30–34].

Particle-mesh Ewald method was used to calculate the electrostatic energy (1 Å grid spacing for three-dimensional fast Fourier transform) [35]. The cutoff for van der Waals interactions was equal to 12 Å. The initial configuration of all systems was obtained after 20 ps NVT simulation. The $Np_N\gamma T$ simulations with 2 fs time steps were carried out for another 3 ns to let the system reach equilibrium. The analysis was performed for a production run of 100 ps. The normal pressure, temperature, and surface tension were set to 1 atm, 20 °C, and 5 mN m^{-1}, respectively. This value of surface tension corresponds to the condensed states of monolayers in which the intermolecular interactions are strong. The intramolecular motions involving hydrogen atoms were frozen during the simulation [36]. The geometry of CHOL and β-$Mal_3O(C_{16+4})_2$ molecules was taken from quantum-chemical calculations (B3LYP/6-31 G*). In both hydrophobic chains of β-$Mal_3O(C_{16+4})_2$ molecule, *all-trans* configuration was forced and was used to prepare the starting configuration of the monolayer.

3. Results and discussion

The structures and models of β-$Mal_3O(C_{16+4})_2$ and CHOL are depicted in Fig. 1.

3.1. Compression isotherms and Brewster angle microscopy

To investigate the interactions between glycolipid and cholesterol, the compression isotherms of pure lipids and their mixtures were recorded at various compositions. Fig. 2 presents the Π-*A* (panel A) and Δ*V*-*A* (panel B) isotherms of β-$Mal_3O(C_{16+4})_2$/CHOL monolayers spread on pure water at 20 °C. The collapse parameters of the isotherms e. g. collapse pressure, Π_{coll}, collapse area, A_{coll}, and surface potential, ΔV_{coll}, as well as the maximum values of compressibility modulus, C_S^{-1} (see Materials and methods section), are listed in Table 1.

The Π-*A* isotherm of β-$Mal_3O(C_{16+4})_2$ has been published previously [18]. This glycolipid forms stable, liquid expanded type monolayer at the air–water interface. The Δ*V*-*A* isotherm (Fig. 2B) shows a number of distinct regions corresponding to a particular phase of the film. The gas phase is formed at areas above 133 $Å^2$ and $\Delta V = 0$ V. Upon compression, ΔV increases up to 0.2 V indicating reorientation of the molecules, which is associated with a gas–liquid expanded phase transition followed by the liquid expanded phase. The highest value of ΔV corresponds to the maximum packing of molecules in the monolayer and the collapse of the film.

The fluid-like character of β-$Mal_3O(C_{16+4})_2$ monolayer was also observed using Brewster angle microscopy (Fig. 3A and B). The BAM image 3A, taken at the gas–liquid expanded phase transition observed in the Δ*V*-*A* isotherm, shows a characteristic foam. At higher surface

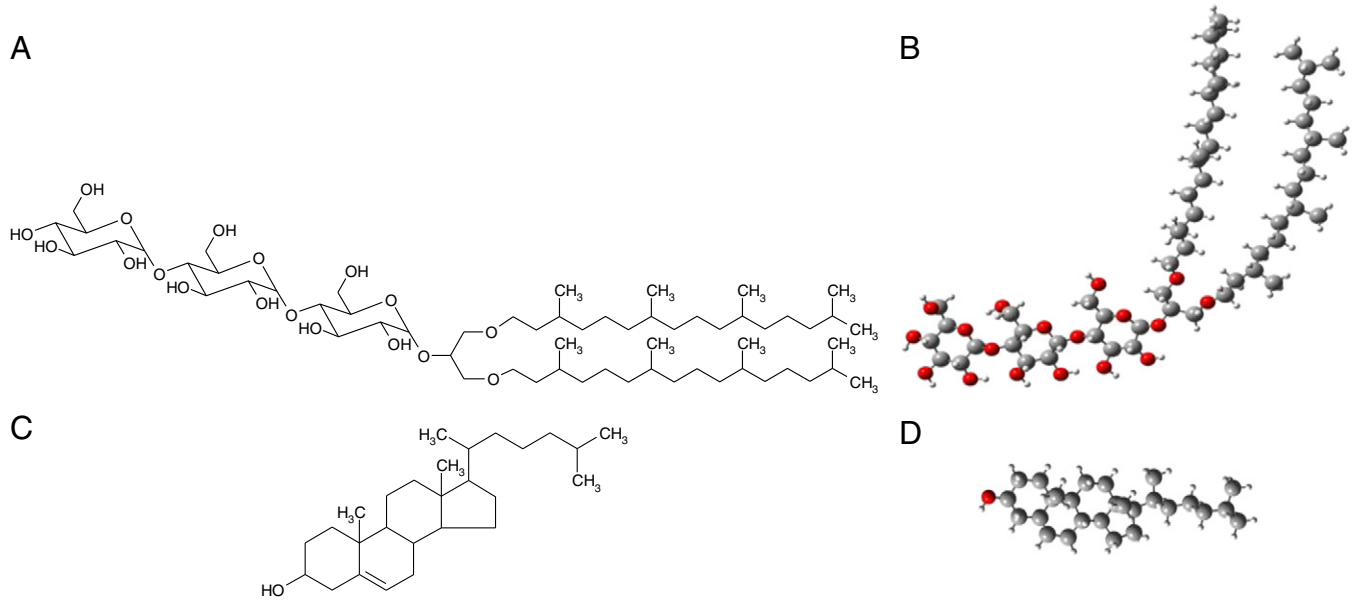

Fig. 1. Structures of β-$Mal_3O(C_{16+4})_2$: (A, B) and CHOL: (C, D). (A, C) chemical structures, and (B, D) geometrical structures obtained at B3LYP/6-31G* level of theory. Color code: carbons in gray, oxygens in red, hydrogens in light gray.

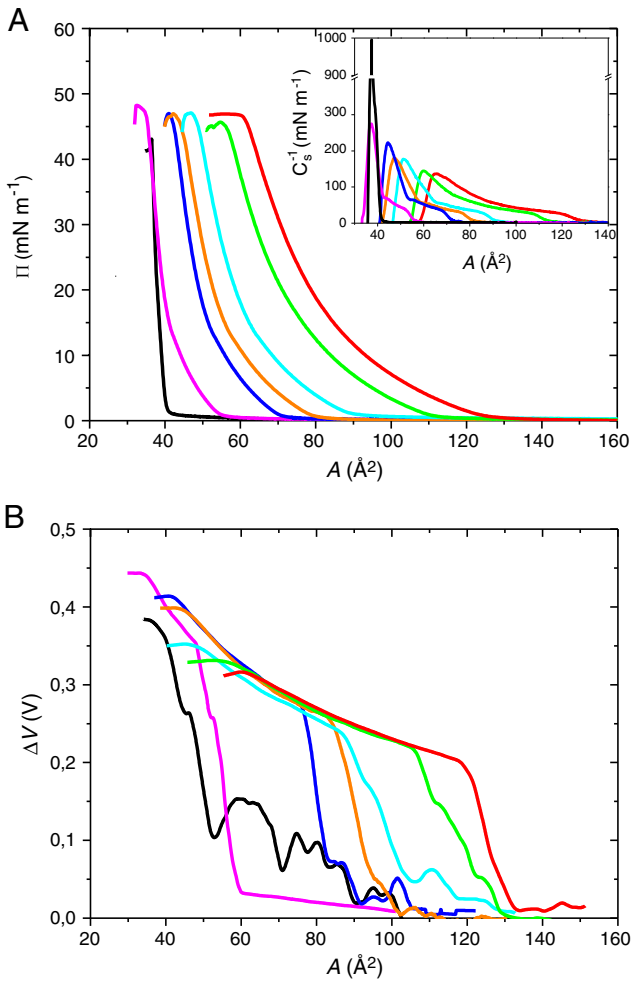

Fig. 2. Π-*A* (A) and Δ*V*-*A* (B) isotherms of binary mixtures β-$Mal_3O(C_{16+4})_2$/CHOL spread on pure water at 20 °C. Red curve: $x_{CHOL}=0$; green curve: $x_{CHOL}=0.2$; cyan curve: $x_{CHOL}=0.4$; orange curve: $x_{CHOL}=0.5$; blue curve: $x_{CHOL}=0.6$; magenta curve: $x_{CHOL}=0.8$; black curve: $x_{CHOL}=1$. Inset: compressibility analysis of monolayers.

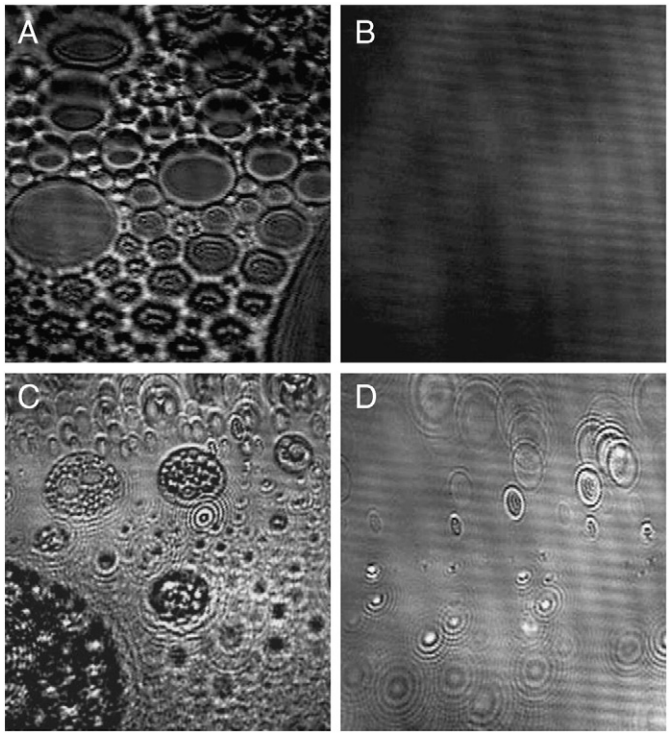

Fig. 3. Brewster angle micrographs of pure monolayers of β-$Mal_3O(C_{16+4})_2$: (A, B) and CHOL: (C, D). The micrographs (A, C) were taken at Π close to 0 mN m^{-1}, $A=130$ and 60 $Å^2$ for (A) and (C) respectively; (B, D): $\Pi=30$ mN m^{-1}. Scale: the width of the snapshots corresponds to 200 μm.

pressure the glycolipid monolayer is isotropic (Fig. 3B); the latter is in accordance with the Π-*A* and Δ*V*-*A* isotherm characteristics.

The compression isotherm of pure cholesterol is in accordance with highly condensed monolayers reported in the literature [37]. The BAM image of the pure CHOL film shows a gas–condensed phase transition (Fig. 3C). The brightness of the images in Fig. 3C and D reflects a higher condensation of these monolayers compared to the respective monolayers of the glycolipid. Above the collapse point (Table 1), aggregates are observed in the pure CHOL film (Fig. 3D).

As shown in Fig. 2A, the surface pressure isotherms of the mixed films are situated between those corresponding to the pure lipid monolayers. The increase of CHOL mole fraction results in a shift of the isotherm toward smaller molecular areas. A significant shift to small areas is observed at the collapse of the monolayers (Table 1). Moreover, the shape of the isotherms of the mixed films depends on the monolayer composition. The isotherm of the $x_{CHOL}=0.2$ mixture is similar to that of the pure glycolipid monolayer; the isotherms with $x_{CHOL}>0.2$ exhibit a steeper slope, systematically increasing with the increase of the cholesterol content in the mixtures. The physical state of the mixed monolayers can be evaluated by the compressibility modulus. According to Davies and Rideal, [22] the C_S^{-1} values 12.5–100 mN m^{-1} and 100–250 mN m^{-1} indicate a liquid expanded and liquid condensed phase, respectively. The inset of Fig. 2A shows a C_S^{-1}-*A* dependency obtained by calculating the first derivative of the Π-*A* isotherms. It can be observed that the liquid expanded phase spans become shorter when x_{CHOL} increases. Indeed, they are observed at 110–70 $Å^2$ and at 52–43 $Å^2$ for $x_{CHOL}=0.2$ and for $x_{CHOL}=0.8$, respectively. In general, the $x_{CHOL}=0.8$ film is the least compressible (the most condensed) among the mixtures studied, as shown in Fig. 2A. On the other hand, the latter system has the highest ordering, as indicated by the highest surface potential values measured at the collapse point (Fig. 2B and Table 1). In general, the mixed β-$Mal_3O(C_{16+4})_2$/CHOL monolayers are characterized by a higher surface potential than the monolayer of pure β-$Mal_3O(C_{16+4})_2$. The overall results suggest that the increase of CHOL promotes the condensation and ordering in the glycolipid film.

In order to better understand the interaction between β-$Mal_3O(C_{16+4})_2$ and CHOL and get insight into their mixing behavior, mean molecular area (MMA) and mean surface potential (MSP) analysis were performed. A comparison between the MMA and MSP of ideal and experimental mixing as a function of CHOL mole fraction at three surface pressures: 10, 20 and 30 mN m^{-1} is shown in Fig. 4.

Deviation from linearity of MMA and MSP occurs for all investigated mixtures and surface pressures. Together with the

Table 1
Characteristic parameters of β-$Mal_3O(C_{16+4})_2$/CHOL isotherms at 20 °C.

x_{CHOL}	A_{coll} ($Å^2$)	Π_{coll} (mN m^{-1})	ΔV_{coll} (V)	$C_{S^{-1}}$ (mN m^{-1})
0	65	38.9	0.29	136.7
0.2	60	37.7	0.32	144.8
0.4	51	38.5	0.34	177.3
0.5	47	35.2	0.39	180.1
0.6	44	36.9	0.40	223.1
0.8	39	33.5	0.42	275.0
1	38	25.9	0.38	994.1

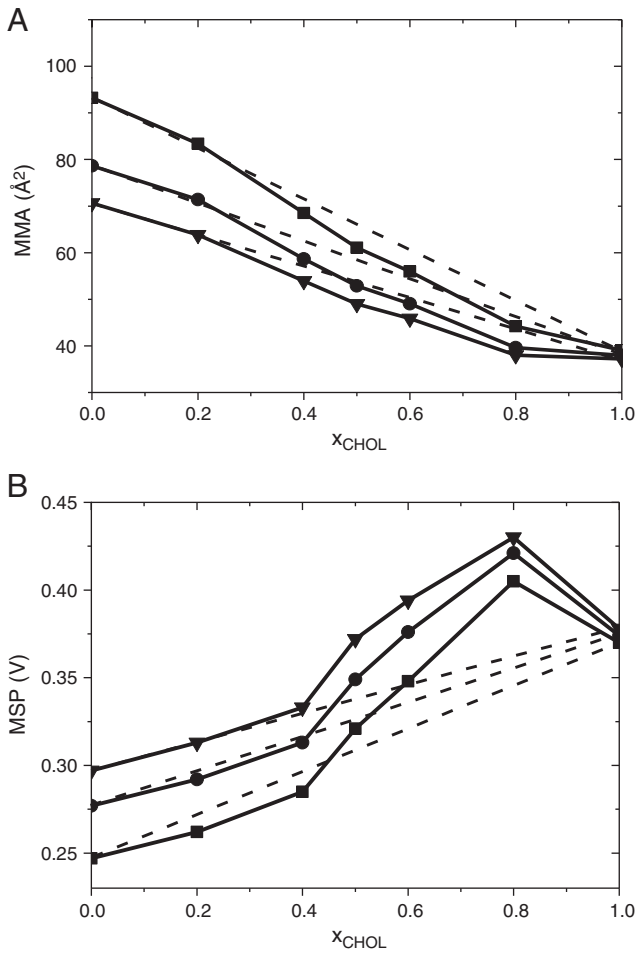

Fig. 4. Miscibility analysis (MMA-x_{CHOL}, A; MSP-x_{CHOL}, B) of β-$Mal_3O(C_{16+4})_2$/CHOL monolayers at Π = 10 (■), 20 (●) and 30 mN m^{-1} (▼). Temperature: 20 °C. The straight lines represent the additive mixing.

collapse pressure criterion [38] shown in Π_{coll} variation with monolayer composition (Table 1), it can be interpreted in terms of miscibility between the two lipids in the Langmuir films. Adding a small amount of CHOL ($x_{CHOL} = 0.2$) to a pure glycolipid matrix leads to a decrease of MMA and an increase of MSP. As a result, a small positive deviation from the ideal MMA value and a negative deviation from MSP are observed; these deviations are well seen at Π = 10 mN m^{-1} (Fig. 4A and B). It indicates a monolayer expansion and disordering of the molecules in the binary mixture compared to the pure lipid films. At higher surface pressure, when the film is more compressed, the deviation becomes negligible. With increasing mole fraction of CHOL ($x_{CHOL} > 0.2$) the MMAs significantly decrease and the deviation from linearity becomes negative. On the contrary, MSP increases and the mixtures with $x_{CHOL} > 0.4$ exhibit large positive deviations. The dependencies obtained suggest that at this concentration cholesterol affects the conformation and packing of the glycolipid hydrocarbon chains, as well as the glycolipid head group interaction, which leads to the condensation of the monolayer and a more upright orientation of the molecules in the mixed monolayer; the latter effect is more significant in the mixtures with higher x_{CHOL} and at higher surface pressures.

The Π-*A* isotherms allowed calculating the Gibbs energy of mixing, ΔG^{ex} (Eq. (2), Materials and methods section). The ΔG^{ex} dependence on composition of the mixed β-$Mal_3O(C_{16+4})_2$/CHOL monolayers, at arbitrary chosen surface pressures, is presented in Fig. 5.

The results obtained were analyzed in terms of the interaction and the mixing behavior of the pure lipids in the film. The deviations from

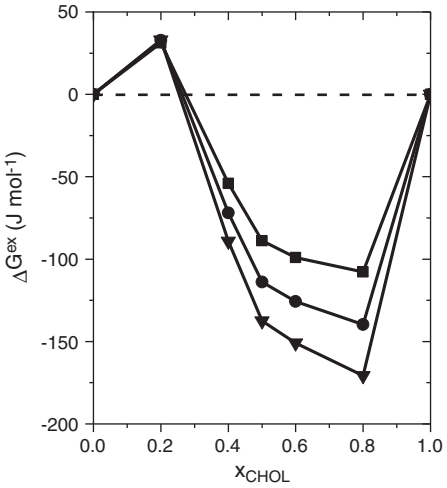

Fig. 5. Gibbs energy of mixing as a function of x_{CHOL}, calculated at Π = 10 (■), 20 (●) and 30 mN m^{-1} (▼). Temperature: 20 °C.

$\Delta G^{ex} = 0$ shown in Fig. 5 support the proposal that the two lipids may form a homogenous phase and are miscible at the investigated compositions. The negative Gibbs energy of mixing observed at $x_{CHOL} > 0.2$ indicates that the interaction between two different lipids is favored compared to interaction between molecules of the same structure. This effect results in an enhanced stability of the monolayers. Maximum stability of the mixed monolayers was reached at $x_{CHOL} = 0.8$. At a lower CHOL content ($x_{CHOL} \leq 0.2$), the ΔG^{ex} is positive, as expected for intermolecular repulsion. Thus, the presence of small amount of CHOL may generate weak steric forces destabilizing the film. For $x_{CHOL} > 0.2$, the observed deviations increase with increasing surface pressure.

The structure of the binary monolayers was monitored by Brewster angle microscopy. BAM images of mixed films investigated at 20 °C are shown in Fig. 6.

BAM images of CHOL/β-$Mal_3O(C_{16+4})_2$ and of pure β-$Mal_3O(C_{16+4})_2$ monolayers (Fig. 3A and B) show that CHOL has a condensing effect. Indeed, while the $x_{CHOL} = 0.2$ and the pure β-$Mal_3O(C_{16+4})_2$ monolayer images (Fig. 6A) indicate a homogenous, isotropic film, the images of mixtures with higher CHOL fractions (Fig. 6B–E) reveal an anisotropic morphology, with circular domains varying in size and number. As the mole fraction of CHOL increases, the bright structures become smaller and more numerous. At the highest CHOL mole fraction the domains become irregular in shape and tend to coalesce in large spots (Fig. 6E). It can be expected that the circular domains are the consequence of lipid mixing and of the ordering of their alkyl chains.

3.2. PM-IRRAS spectra

To gain more insight into the glycolipid–cholesterol interaction at a molecular level, spectroscopic studies were performed. To this end, polarization-modulation infrared reflection-absorption spectroscopy [39,40] was employed to investigate the interaction between the molecules in one- and two-component monomolecular films.

First, IR transmittance spectra of CHOL and β-$Mal_3O(C_{16+4})_2$ have been measured (Fig. 7). The IR bands are displayed in two spectral ranges: 3000–2800 and 1500–1000 cm^{-1}.

The peaks observed in the 3000–2800 region can be assigned to CH_3 and CH_2 stretching vibrations. The strong CH_2 asymmetric and symmetric stretching [$\nu_{as}(CH_2)$ and $\nu_s(CH_2)$, respectively] and less intense signals corresponding to CH_3 asymmetric and symmetric stretch [$\nu_{as}(CH_3)$ and $\nu_s(CH_3)$, respectively] were observed for both molecules. The values of the characteristic vibrations of the spectra are given in Table 2. The most intense band observed in the spectrum

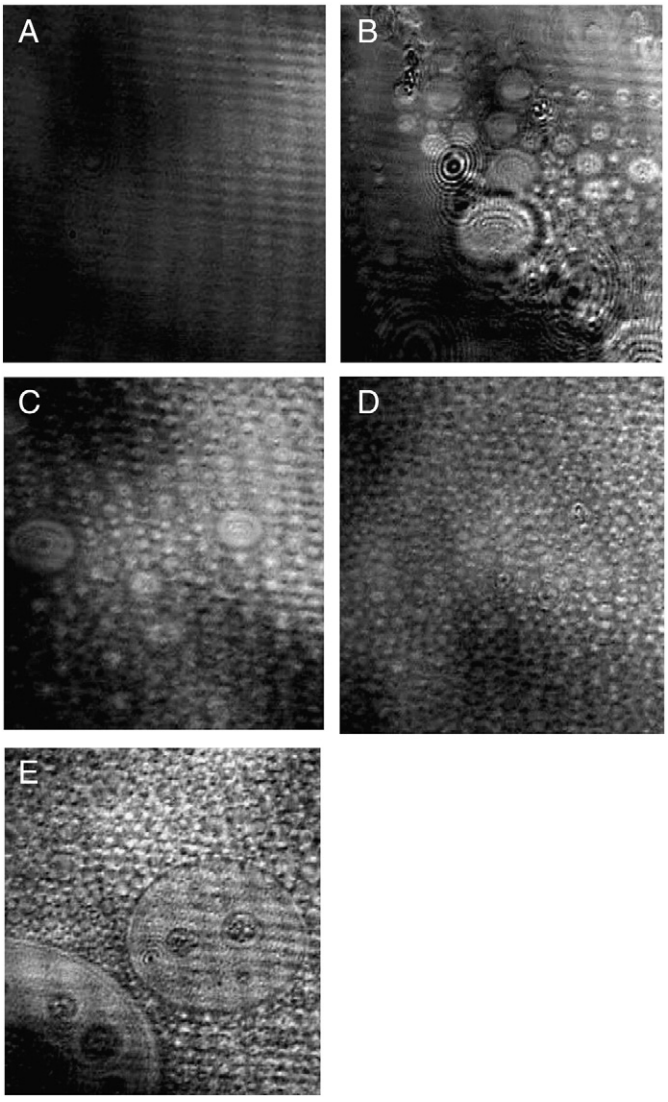

Fig. 6. Brewster angle micrographs of β-$Mal_3O(C_{16+4})_2$/CHOL mixed monolayers. (A): $x_{CHOL}=0.2$; (B): $x_{CHOL}=0.4$; (C): $x_{CHOL}=0.5$; (D): $x_{CHOL}=0.6$; (E): $x_{CHOL}=0.8$. The micrographs were taken at $\Pi=5$ mN m^{-1}. Scale: the width of the snapshots corresponds to 200 μm.

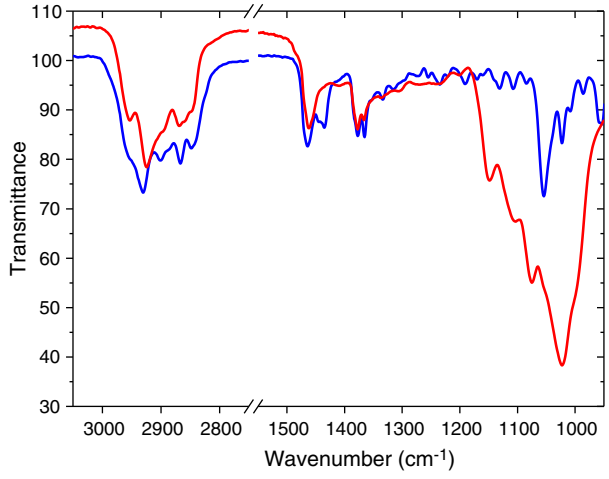

Fig. 7. IR transmittance spectra of β-$Mal_3O(C_{16+4})_2$ (red) and CHOL (blue).

Table 2
Characteristic vibrational wavenumbers of β-$Mal_3O(C_{16+4})_2$ and CHOL bands in the pure and mixed systems obtained from transmittance IR and PM-IRRAS spectra.

x_{CHOL}	$\nu_{as}(CH_3)$ (cm^{-1})	$\nu_{as}(CH_2)$ (cm^{-1})	$\nu_s(CH_3)$ (cm^{-1})	$\nu_s(CH_2)$ (cm^{-1})	$\delta_{as}(C–CH_3)$ (cm^{-1})	$\delta_s(C–CH_3)$ (cm^{-1})	$\nu(C–O)$ (cm^{-1})
IR transmittance spectra							
0	2953	2924	2869	2851	1462	1377, 1366	1023
1	2953	2930	2867	2847	1464	1377, 1365	1054
PM-IRRAS spectra							
0	2959	2920	2864	2848	1453	1392, 1364	1045
0.2	2967	2926	2886	2859	1454	1385, 1360	1046
0.8	2958	2915	2875	2832	1478	1371, 1387	1047
1	2948	2917	2866	2827	1466	1402, 1376	1069

at 1023 and 1054 cm^{-1}, for β-$Mal_3O(C_{16+4})_2$ and CHOL respectively, can be associated with the alcohol C–O stretching [ν(C–O)]. C–CH_3 asymmetric and symmetric bending vibrations [$\delta_{as}(C–CH_3)$ and $\delta_s(C–CH_3)$] are present in the spectra as well. The symmetric band, known as umbrella mode, is split into two frequencies, which is indicative of the methyl branching of the glycolipid and cholesterol alkyl chains.

The PM-IRRAS spectra of pure and mixed monomolecular films were recorded on water subphase at surface pressure of 30 mN m^{-1}. The spectra obtained with pure β-$Mal_3O(C_{16+4})_2$, pure CHOL and mixed $x_{CHOL}=0.2$ or $x_{CHOL}=0.8$ films are shown in Fig. 8.

PM-IRRAS was used for studying glycolipids in Langmuir films [41]. PM-IRRAS spectra of pure Langmuir films exhibit characteristic vibrations of lipids identified in the IR spectra. The changes in the band position observed in the PM-IRRAS spectra (Table 2) can be ascribed to the optical properties of water subphase and to the orientation of the alkyl chains [42].

Application of PM-IRRAS to the two-component monolayer study gives us reliable information on miscibility at the air–water interface. Indeed, the characteristic frequencies measured for mixed monolayers are different than those measured for pure lipid films. Fig. 8 clearly demonstrates that the spectrum of β-$Mal_3O(C_{16+4})_2$ is altered by cholesterol. According to the Crisp phase rules, [38] it indicates interaction and, consequently, miscibility between β-$Mal_3O(C_{16+4})_2$ and CHOL. Indeed, in the case of completely immiscible species that is in the absence of interaction between the two lipids, spectral bands characteristic for pure lipids would be observed.

The C–H stretching region (Fig. 8A) can be used to monitor the structural order of the hydrocarbon chains. The asymmetric and symmetric stretching vibrations of methylene group, which typically appear around 2920 and 2850 cm^{-1}, respectively, are particularly valuable in this respect. A redshift of the $\nu_{as}(CH_2)$ and $\nu_s(CH_2)$ bands indicates higher chain ordering (*all trans* conformation) in the film, while a blueshift suggests chain disordering (*gauche* conformation) [43]. In the PM-IRRAS spectrum of pure CHOL film these bands show, respectively, at 2917 and 2827 cm^{-1}, which indicates high conformational ordering of the short alkyl chains. In the case of β-$Mal_3O(C_{16+4})_2$, $\nu_{as}(CH_2)$ and $\nu_s(CH_2)$ are observed at 2920 and 2848 cm^{-1}, respectively, suggesting that the β-$Mal_3O(C_{16+4})_2$ phytanyl chains are less ordered and more tilted compared to CHOL; this result is consistent with the compression isotherm experiments showing a more fluid-like character of the former lipid film. In the case of the $x_{CHOL}=0.2$ and $x_{CHOL}=0.8$ mixed films, the CH_2 bands appear at, respectively, 2926 and 2859 cm^{-1}, and at 2915 and 2832 cm^{-1}. The effect reflects conformational disordering of hydrocarbon chains in the presence of small amounts of cholesterol and, on the contrary, higher ordering in the presence of higher amounts of cholesterol. A similar effect is observed in the case of $\nu_{as}(CH_3)$ and $\nu_s(CH_3)$ bands. The lower wavenumbers observed in the case of CHOL-rich mixture compared to the CHOL-poor mixture indicate formation of a more rigid and closely packed monolayer in the former case.

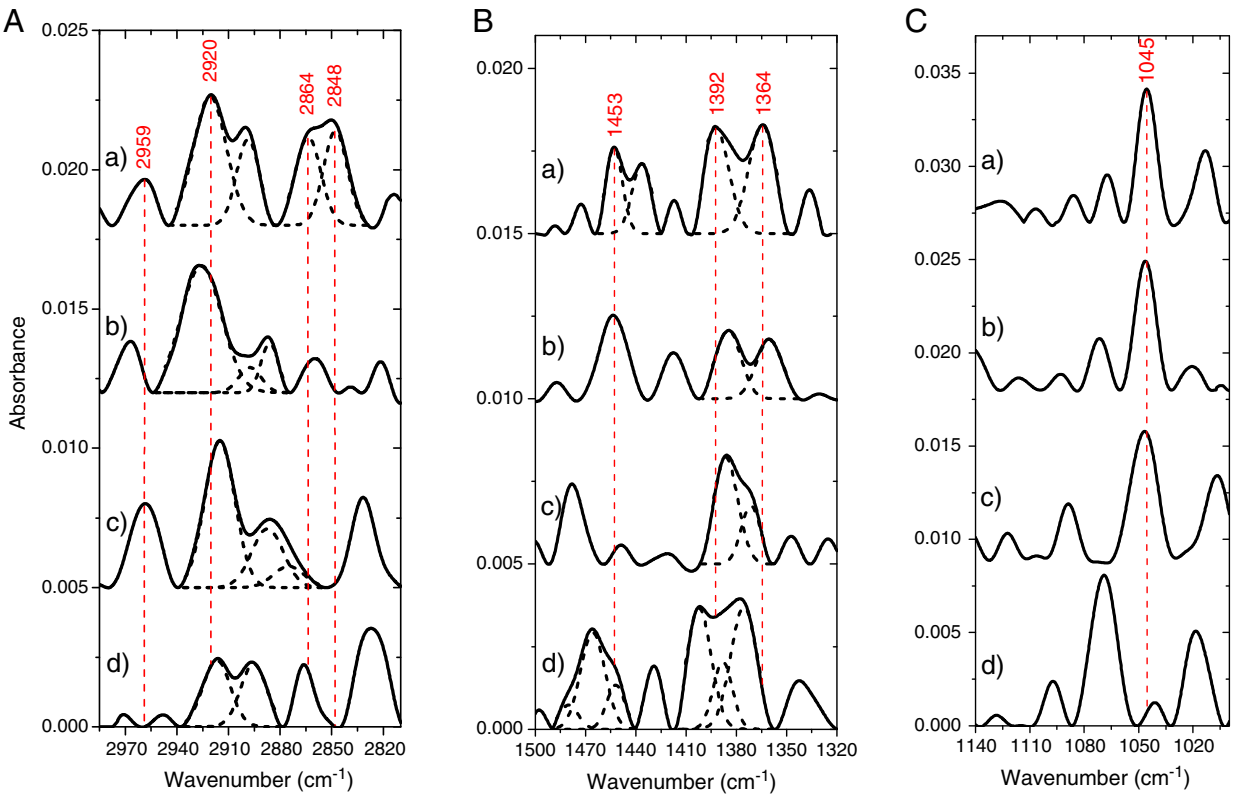

Fig. 8. PM-IRRAS spectra of the pure and mixed β-$Mal_3O(C_{16+4})_2$/CHOL monolayers taken at 30 mN m^{-1}. (A) CH_3 and CH_2 stretching region; (B) C–CH_3 bending region; (C) alcohol C–O stretching region. Pure β-$Mal_3O(C_{16+4})_2$ (a), $x_{CHOL}=0.2$ (b), $x_{CHOL}=0.8$ (c), and pure CHOL (d). Solid lines: experimental spectra; dashed lines: deconvoluted bands.

The most useful band for studying molecular interaction in the CHOL and β-$Mal_3O(C_{16+4})_2$ films is the C–O stretching vibration observed in the fingerprint region (Fig. 8C). Importantly, the position of ν(C–O) is sensitive to hydrogen bonding. As reported in the literature, for groups involved in hydrogen bonding to water, the stretching mode absorption bands shift to lower frequency, whereas bending mode absorption bands shift to higher frequency, as H-bonding increases and temperature decreases [44]. In our experiments, the ν(C–O) band is observed at 1045 cm^{-1} and at 1069 cm^{-1}, respectively, for the pure films formed with β-$Mal_3O(C_{16+4})_2$ or CHOL. These results indicate that a hydrogen bond network is formed between the sugar maltooligosaccharide headgroups, which are less hydrated, compared to the cholesterol –OH. Interestingly, the introduction of CHOL into the β-$Mal_3O(C_{16+4})_2$ film results in a slight increase in ν(C–O) frequencies (Table 2). The corresponding bands occur at 1046 cm^{-1} for $x_{CHOL}=0.2$ and 1047 cm^{-1} for $x_{CHOL}=0.8$. These results indicate that the differences in hydrogen bonding between the two mixtures are rather small, even though the composition of the mixtures is quite different. In both mixtures, the head group region participates in intermolecular hydrogen bonding which can be expected to stabilize the two-component films. On the other hand, a significant redshift of the ν(C–O) stretching band from 1069 to 1047 cm^{-1} is observed when adding a small amount of β-$Mal_3O(C_{16+4})_2$ to pure CHOL film; this may suggest that, in the mixed film, the cholesterol –OH involves preferentially in hydrogen bonding with the maltooligosaccharide headgroups rather compared to interaction with water.

The C–CH_3 asymmetric and symmetric bending frequencies are useful for the β-$Mal_3O(C_{16+4})_2$/CHOL film study as well; these bands are observed between 1478 and 1360 cm^{-1} (Table 2 and Fig. 8B). The C–CH_3 bending frequencies in $x_{CHOL}=0.2$ film are similar [δ_{as}(C–CH_3)] or lower [δ_s(C–CH_3)] compared to the pure β-$Mal_3O(C_{16+4})_2$ film, and go higher for $x_{CHOL}=0.8$; the only exception in the latter case is δ_s (C–CH_3) band observed at 1371 cm^{-1}. This result is in accordance with the results obtained for the CH_2 and CH_3 stretching vibrations, and supports a higher ordering of the alkyl chains in the mixture with the higher content of cholesterol.

3.3. Molecular dynamics simulation

Molecular dynamic calculations complement experimental measurements and provide atomic-level information about the monolayer. In Fig. 9 and 10, the configuration of the system at the end of simulation is shown for pure and mixed monolayers, respectively. The CHOL monolayer (Fig. 9A; side view) shows that molecules are tilted with respect to the water surface. To estimate the tilt angle, a vector linking the carbon atoms substituted by –OH and $-C_8H_{17}$ moieties was used. The obtained values are collected in Table 3.

For the pure CHOL monolayer the tilt angle (ϑ) is 13° and increases with increasing β-$Mal_3O(C_{16+4})_2$ contents. It is well seen in the top view snapshots ($x_{CHOL}=1.0$ or 0.8 plots compared to $x_{CHOL}=0.2$). The projection of CHOL molecule geometry onto the *xy* plane in mixed monolayers is longer compared to the projection in pure CHOL monolayer. In the case of β-$Mal_3O(C_{16+4})_2$, the tilt vector was defined by the first and the last carbon atom in both chains. The obtained average tilt angles are collected in Table 3. The tilt angle decreases with the increasing CHOL contents. Interestingly, the tilt angle of the β-$Mal_3O(C_{16+4})_2$ chains is comparable for the two mixed films, while the CHOL tilt angle is much lower in the $x_{CHOL}=0.8$ than in $x_{CHOL}=0.2$ film. The latter indicates that the condensed domains are predominantly composed of ordered CHOL molecules, with β-$Mal_3O(C_{16+4})_2$ molecules forming the expanded phase. It is also

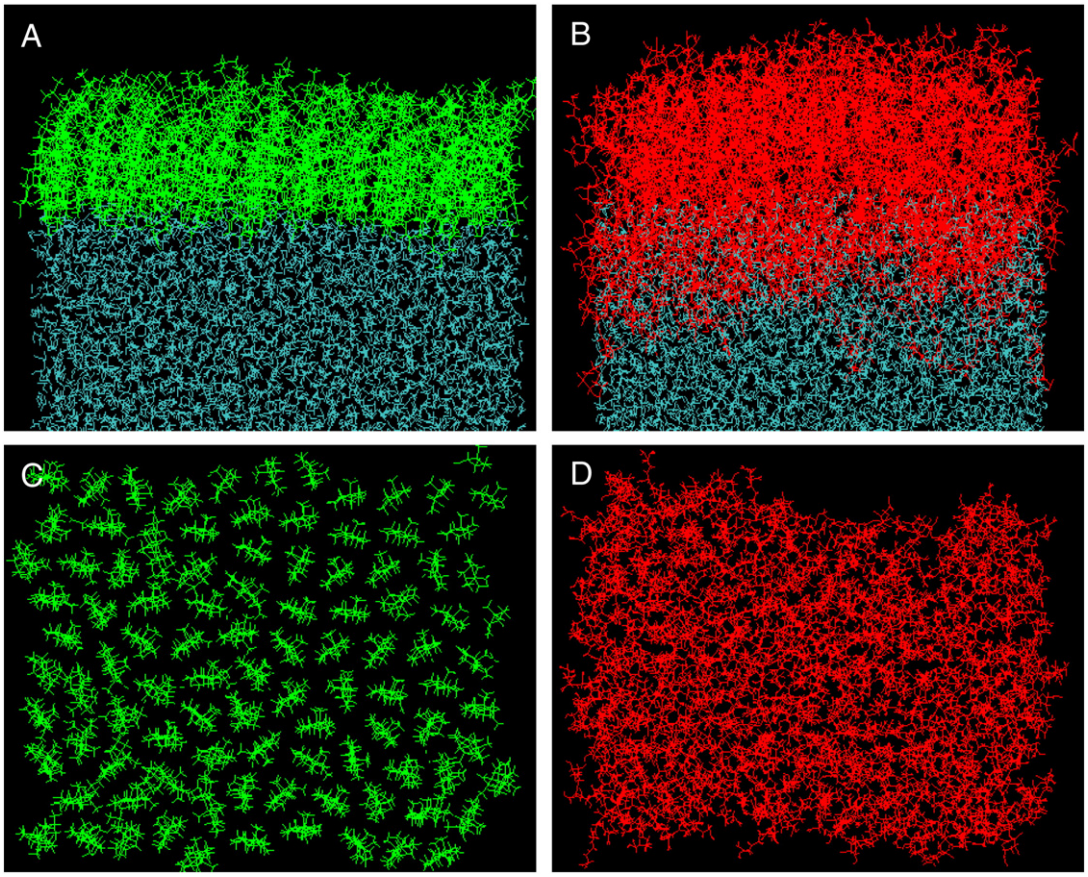

Fig. 9. Snapshots from the simulation of CHOL (A, C) and β-$Mal_3O(C_{16+4})_2$ (B, D) monolayers. First and second rows: side (A, B) and top (C, D) views, respectively. Color code: CHOL, green; β-$Mal_3O(C_{16+4})_2$, red; water, blue.

worth noticing that the high tilt angle of CHOL in the $x_{CHOL}=0.2$ film explains the fluidity of the film observed in the BAM image (Fig. 6A).

One more observation coming from the top-view snapshots is the lost of rotational order of the tilt vector. The average value of rotational order parameter is zero for the CHOL monolayer.

$$g = < 2\ \cos^2(\varphi) - 1 >$$

where φ is the azimuthal angle of the tilt vector. The zero value indicates a complete disorder in the orientation while the ± 1 value indicates a perfect ordering. Similarly to CHOL, the average rotational order parameters of β-$Mal_3O(C_{16+4})_2$ molecules are close to zero, indicating disorder in orientation in the *xy* plane. Another parameter characterizing the hydrophobic part of β-$Mal_3O(C_{16+4})_2$ molecule is the average order parameter,

$$S = \left(3 < \cos^2\theta > -1\right)/2,$$

where θ refers to the successive dihedral angles in the carbon skeleton. $S=1.0$ indicates that all carbon atoms in the chain are in *all trans* conformation while total disorder in the chain corresponds to $S=0.0$. The computed values of S are listed in Table 3. It can be observed that with increasing cholesterol contents the average order parameter increases. In other words, cholesterol influences ordering in hydrocarbon chains. The ordering effect of CHOL was observed in the PM-IRRAS spectra as well.

Molecular dynamics simulations give information about the degree of hydration of polar heads. Indeed, the radial distribution function ($G_{X-(OH_2)}(r)$) is a useful quantity to describe the structure of headgroups and their association with water molecules. Fig. 11 shows the evolution of $G_{X-(OH_2)}(r)$ profiles with the molar ratio; X corresponds to hydroxyl oxygen atoms in CHOL, hydroxyl oxygen atoms in β-$Mal_3O(C_{16+4})_2$, linker oxygen atoms in β-$Mal_3O(C_{16+4})_2$, and ring oxygen atoms (Fig. 11A–D, respectively).

It can be seen that with increasing $Mal_3O(C_{16+4})_2$ content the height of the first peak decreases (Fig. 11A). The position of this peak does not depend on the CHOL mole fraction. Hydroxyl oxygens of CHOL are more hydrated in pure CHOL monolayer than in mixed β-$Mal_3O(C_{16+4})_2$/CHOL films. These findings are consistent with the PM-IRRAS results, which show a redshift of the ν(C–O) frequency in the mixed monolayers compared to pure CHOL. The opposite behavior is observed for hydroxyl oxygens in β-$Mal_3O(C_{16+4})_2$ (Fig. 11B). Indeed, the intensity of the first peak of the pure β-$Mal_3O(C_{16+4})_2$ monolayer is lower than in the mixed films, as a result of lower hydration of this layer. In accordance with the spectroscopic study, the hydration of different mixtures is comparable; the peak corresponding to $x_{CHOL}=0.2$ is only slightly lower than that of $x_{CHOL}=0.8$. It may be the consequence of the bulky maltooligosaccharide headgroups of β-$Mal_3O(C_{16+4})_2$ that block the space around the hydroxyl group of CHOL and reduce the accessibility of water molecules in both mixtures. The lowest influence of CHOL mole fraction is observed for the linker oxygen atoms in β-$Mal_3O(C_{16+4})_2$ (Fig. 11C). Due to an important steric hindrance of sugar residues at both sides of the linker oxygens the first coordination shell is practically unaffected by CHOL contents. The differences are pronounced in the second coordination shell. Radial distribution function for ring oxygens (Fig. 11D), namely intensity and

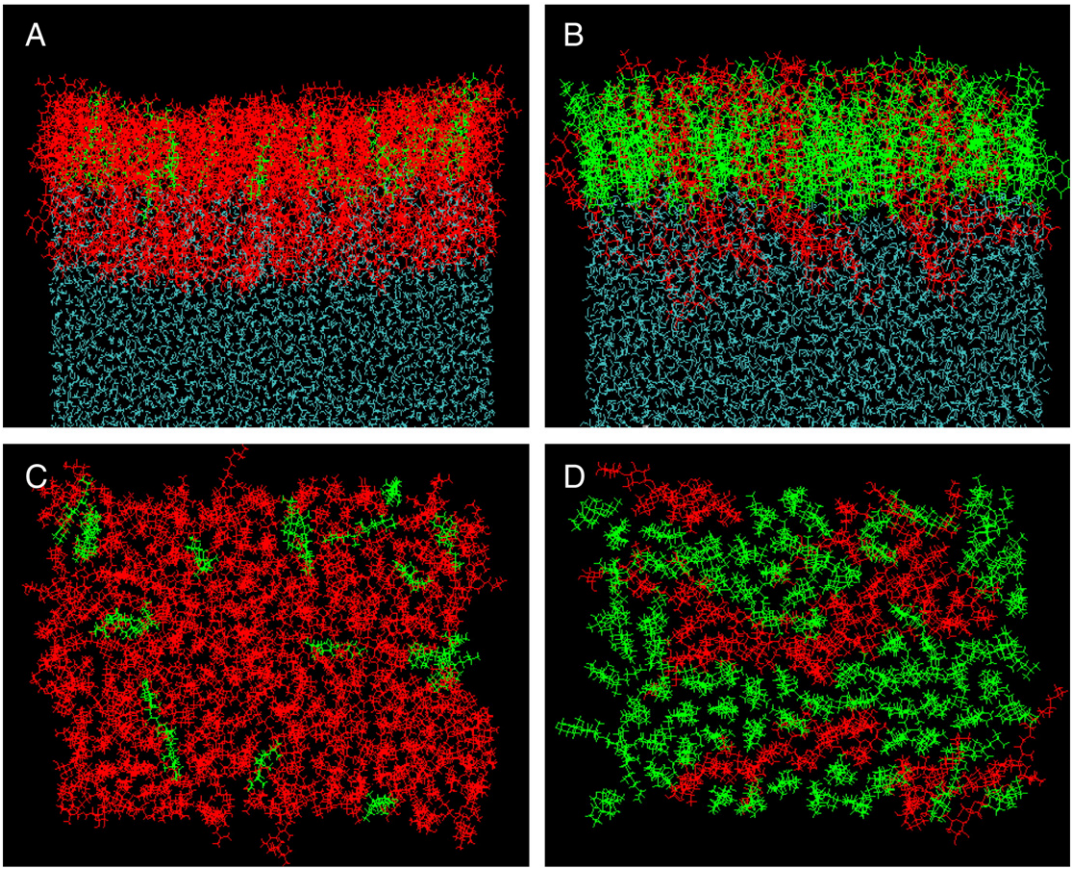

Fig. 10. Snapshots from the simulation of β-$Mal_3O(C_{16+4})_2$/CHOL mixed films at the air–water interface: $x_{CHOL} = 0.2$ (A, C) and $x_{CHOL} = 0.8$ (B, D). (A, B) side and (C, D) top views. Color code: CHOL, green; β-$Mal_3O(C_{16+4})_2$, red.

location of the first peak for the low CHOL content is the same as for high CHOL content; in the pure β-$Mal_3O(C_{16+4})_2$ monolayer the intensity of the first peak is higher.

4. Conclusions

The properties of phytanyl-chained glycolipid/cholesterol monolayers were studied experimentally and theoretically. The results obtained show that the presence of cholesterol in glycolipid films yields condensed phase domains with a highly organized molecular arrangement. The size and total area of the domains depended on the cholesterol concentration; more rigid and ordered packing of lipid molecules were observed in the case of the films with higher concentration of cholesterol.

PM-IRRAS studies and molecular dynamics simulations gave us more insight in the structural rearrangement of the glycolipid chains, and in glycolipid–cholesterol interaction in the polar head region with increasing x_{CHOL}. The increasing film condensation with increasing x_{CHOL} shows as a decrease of C–H stretching frequencies in the PM-IRRAS spectra. This redshift can be interpreted in terms of a higher degree of ordering and a higher number of *all trans* conformations. The frequency increase observed for $x_{CHOL} = 0.2$ reflects chain disordering and prevalence of *gauche* conformations. These observations are in accordance with BAM results and with theoretical calculations; the latter show that β-$Mal_3O(C_{16+4})_2$ chains are more tilted than the chains of CHOL. The increase of x_{CHOL} leads to a decrease in the tilt angle of the phytanyl chains. Interestingly, the CHOL tilt angle is different for different mixtures; it is lower for lower concentrations of the glycolipid. Consequently, we propose that formation of domains is driven by chain ordering of both cholesterol and glycolipid.

Moreover, spectroscopic measurements and molecular dynamics calculations showed a strong propensity of the maltooligosaccharide headgroup to hydrogen bonding. The hydrogen bonding between the maltooligosaccharide and cholesterol hydroxyl groups revealed in our study is of particular interest. Indeed, this stabilizing interaction could be used in elaborating lipid systems for drug delivery and other applications.

Table 3
The average tilt angles (ϑ), rotational order parameters (g), order parameter (S) and area per molecule (A) obtained from molecular dynamics simulations.

x_{CHOL}	ϑ_{CHOL} (°)	g_{CHOL}	$\vartheta_{\beta\text{-}Mal_3O(C_{16+4})_2}$ (°)	$g_{\beta\text{-}Mal_3O(C_{16+4})_2}$	S
0	–	–	45	−0.01	0.38
0.2	35	0.00	28	−0.01	0.44
0.8	18	0.00	26	−0.15	0.58
1	13	0.00	–	–	–

Acknowledgments

This work was supported by the Ministry of Science and Higher Education, Poland (project no. 1206/GDR/2007/03) within the framework of French-Polish collaboration, AIST, Japan (Research and Development Projects of Industrial Science and Technology Frontier Program, subject: Physical properties of membrane protein/lipid assemblies) and a Hubert Curien partnership ("Polonium", no.

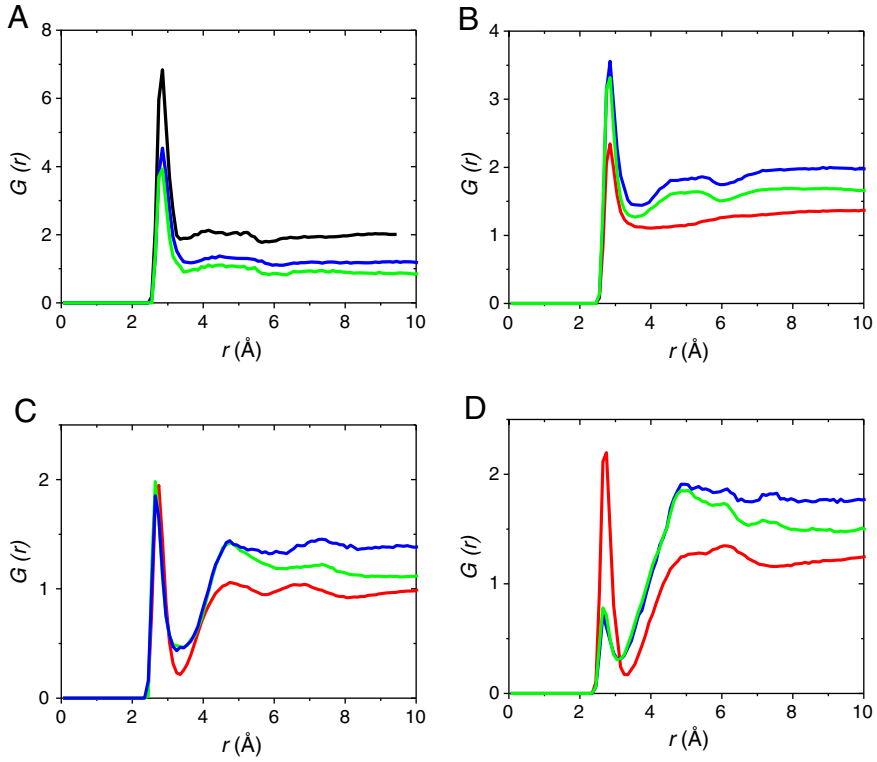

Fig. 11. Radial distribution function of water oxygen atoms around headgroup oxygen atoms *X*, $g_{XO(water)}(r)$: (A) CHOL hydroxyl oxygen atoms, (B) β-$Mal_3O(C_{16+4})_2$ hydroxyl oxygen atoms, (C) β-$Mal_3O(C_{16+4})_2$ oxygen atoms of COC linear junctions and (D) β-$Mal_3O(C_{16+4})_2$ ring oxygen atoms. Black: pure CHOL; red: pure β-$Mal_3O(C_{16+4})_2$; blue: ($x_{CHOL}=0.8$); green: ($x_{CHOL}=0.2$).

20077QA). The authors thank Françis Hoffmann and Eric Dubs for excellent technical assistance. The calculations were carried out with the equipment purchased thanks to the financial support of the European Regional Development Fund in the framework of the Polish Innovation Economy Operational Program (contract no. POIG.02.01.00-12-023/08).

References

[1] S.N. Sehgal, M. Kates, N.E. Gibbons, Lipids of *Halobacterium cutirubrum*, Can. J. Biochem. Physiol. 40 (1962) 69–81.
[2] G.D. Sprott, Structures of archaebacterial membrane lipids, J. Bioenerg. Biomembr. 24 (1992) 555–566.
[3] Y. Koga, H. Morii, Recent advances in structural research on ether lipids from Archaea including comparative and physiological aspects, Biosci., Biotechnol., Biochem. 69 (2005) 2019–2034.
[4] Y. Koga, H. Morii, Biosynthesis of ether-type polar lipids in Archaea and evolutionary considerations, Microbiol. Mol. Biol. Rev. 71 (2007) 97–120.
[5] T. Benvegnu, L. Lemiegre, S. Cammas-Marion, Archaeal lipids: innovative materials for biotechnological applications, Eur. J. Org. Chem. (2008) 4725–4744.
[6] L. Krishnan, G.D. Sprott, Archaeosome adjuvants: immunological capabilities and mechanism(s) of action, Vaccine 26 (2008) 2043–2055.
[7] G.B. Patel, G.D. Sprott, Archaebacterial ether lipid liposomes (Archaeosomes) as novel vaccine and drug delivery systems, Crit. Rev. Biotechnol. 19 (1999) 317–357.
[8] T. Baba, H. Minamikawa, M. Hato, A. Motoki, M. Hirano, D. Zhou, K. Kawasaki, Synthetic phytanyl-chained glycolipid vesicle membrane as a novel matrix for functional reconstitution of cyanobacterial photosystem II complex, Biochem. Biophys. Res. Commun. 265 (1999) 734–738.
[9] V. Borshchevskiy, E. Moiseeva, A. Kuklin, G. Bueldt, M. Hato, V. Gordeliy, Isoprenoid-chained lipid beta -XylOC16+4-A novel molecule for in meso membrane protein crystallization, J. Cryst. Growth 312 3326–3330.
[10] T.G. Tornabene, T.A. Langworthy, G. Holzer, J. Oro, Squalenes, phytanes and other isoprenoids as major neutral lipids of methanogenic and thermoacidophilic "archaebacteria", J. Mol. Evol. 13 (1979) 73–83.
[11] M. Kates, Structure, physical properties, and function of archaebacterial lipids, Prog. Clin. Biol. Res. 282 (1988) 357–384.
[12] M. Kates, Membrane lipids of archaea, New Compr. Biochem. 26 (1993) 261–295.
[13] P.F. Smith, in: C. Ratledge, S.G. Wilkinson (Eds.), Microbial Lipids, Academic Press, London, 1988, pp. 489–553, Vol. 1.
[14] H. Minamikawa, M. Hato, Phase behavior of synthetic phytanyl-chained glycolipid/water systems, Langmuir 13 (1997) 2564–2571.
[15] H. Minamikawa, M. Hato, Reverse micellar cubic phase in a phytanyl-chained glucolipid/water system, Langmuir 14 (1998) 4503–4509.
[16] M. Hato, H. Minamikawa, K. Tamada, T. Baba, Y. Tanabe, Self-assembly of synthetic glycolipid/water systems, Adv. Colloid Interface Sci. 80 (1999) 233–270.
[17] T. Arakawa, S.N. Timasheff, Stabilization of protein structure by sugars, Biochemistry 21 (1982) 6536–6544.
[18] B.M. Korchowiec, T. Baba, H. Minamikawa, M. Hato, Forces that control pH-dependent aggregation of nonionic glycolipid vesicles, Langmuir 17 (2001) 1853–1859.
[19] S. Lund-Katz, H.M. Laboda, L.R. McLean, M.C. Phillips, Influence of molecular packing and phospholipid type on rates of cholesterol exchange, Biochemistry 27 (1988) 3416–3423.
[20] B. Korchowiec, M. Paluch, Y. Corvis, E. Rogalska, A Langmuir film approach to elucidating interactions in lipid membranes: 1,2-dipalmitoyl-sn-glycero-3-phosphoethanolamine/cholesterol/metal cation systems, Chem. Phys. Lipids 144 (2006) 127–136.
[21] B. De Kruyff, R.A. Demel, A.J. Slotboom, L.L.M. Van Deenen, A.F. Rosenthal, Effect of the polar headgroup on the lipid–cholesterol interaction. Monolyaer and differential scanning calorimetry study, Biochim. Biophys. Acta, Biomembr. 307 (1973) 1–19.
[22] J.T. Davies, E.K. Rideal, Interfacial Phenomena, 2nd ed Academic Press, New York, 1963.
[23] F.C. Goodrich, Molecular Interaction in Mixed Monolayers, Proc. Int. Congr. Surf. Act., 2nd 1, 1957, pp. 85–91.
[24] K.J. Bacon, G.T. Barnes, Two-component monolayers. IV. The excess enthalpies and entropies of mixing in the octadecanol-docosyl sulfate system, J. Colloid Interface Sci. 67 (1978) 70–77.
[25] L. Kale, R. Skeel, M. Bhandarkar, R. Brunner, A. Gursoy, N. Krawetz, J. Phillips, A. Shinozaki, K. Varadarajan, K. Schulten, NAMD2: greater scalability for parallel molecular dynamics, J. Comput. Phys. 151 (1999) 283–312.
[26] B.R. Brooks, R.E. Bruccoleri, B.D. Olafson, D.J. States, S. Swaminathan, M. Karplus, CHARMM: a program for macromolecular energy, minimization, and dynamics calculations, J. Comput. Chem. 4 (1983) 187–217.
[27] W.L. Jorgensen, J. Chandrasekhar, J.D. Madura, R.W. Impey, M.L. Klein, Comparison of simple potential functions for simulating liquid water, J. Chem. Phys. 79 (1983) 926–935.
[28] Y. Zhang, S.E. Feller, B.R. Brooks, R.W. Pastor, Computer simulation of liquid/liquid interfaces. I. Theory and application to octane/water, J. Chem. Phys. 103 (1995) 10252–10266.
[29] S.E. Feller, Y. Zhang, R.W. Pastor, Computer simulation of liquid/liquid interfaces. II. Surface tension-area dependence of a bilayer and monolayer, J. Chem. Phys. 103 (1995) 10267–10276.

[30] F. Sun, Constant normal pressure, constant surface tension, and constant temperature molecular dynamics simulation of hydrated 1,2-dilignoceroylphosphatidylcholine monolayer, Biophys. J. 82 (2002) 2511–2519.
[31] M. Pickholz, O.N. Oliveira Jr., M.S. Skaf, Molecular dynamics simulations of neutral chlorpromazine in zwitterionic phospholipid monolayers, J. Phys. Chem. B 110 (2006) 8804–8814.
[32] J. Chanda, S. Bandyopadhyay, Molecular dynamics study of surfactant monolayers adsorbed at the oil/water and air/water interfaces, J. Phys. Chem. B 110 (2006) 23482–23488.
[33] S. Rovillard, E. Perez, R. Ionov, M. Voue, J. De Coninck, Monolayer organization modeling using molecular dynamics, Langmuir 15 (1999) 2749–2754.
[34] S. Baoukina, L. Monticelli, S.J. Marrink, D.P. Tieleman, Pressure–area isotherm of a lipid monolayer from molecular dynamics simulations, Langmuir 23 (2007) 12617–12623.
[35] H.C. Andersen, RATTLE: a "velocity" version of the SHAKE algorithm for molecular dynamics calculations, J. Comput. Phys. 52 (1983) 24–34.
[36] T. Darden, D. York, L. Pedersen, Particle mesh Ewald: an N.cntdot.log(N) method for Ewald sums in large systems, J. Chem. Phys. 98 (1993) 10089–10092.
[37] M. Savva, S. Acheampong, The interaction energies of cholesterol and 1,2-dioleoyl-sn-glycero-3-phosphoethanolamine in spread mixed monolayers at the air–water interface, J. Phys. Chem. B 113 (2009) 9811–9820.
[38] D.J. Crisp, A two-dimensional phase rule II, Some Applications of a Two-Dimensional Phase Rule for a Single Interface, Research (London, 1949, pp. 23–35.
[39] D. Blaudez, T. Buffeteau, J.C. Cornut, B. Desbat, N. Escafre, M. Pezolet, J.M. Turlet, Polarization-modulated FT-IR spectroscopy of a spread monolayer at the air/water interface, Appl. Spectrosc. 47 (1993) 869–874.
[40] D. Blaudez, J.-M. Turlet, J. Dufourcq, D. Bard, T. Buffeteau, B. Desbat, Investigations at the air/water interface using polarization modulation IR spectroscopy, J. Chem. Soc., Faraday Trans. 92 (1996) 525–530.
[41] C. Bottier, J. Gean, F. Artzner, B. Desbat, M. Pezolet, A. Renault, D. Marion, V. Vie, Galactosyl headgroup interactions control the molecular packing of wheat lipids in Langmuir films and in hydrated liquid-crystalline mesophases, Biochim. Biophys. Acta, Biomembr. 1768 (2007) 1526–1540.
[42] R. Mendelsohn, J.W. Brauner, A. Gericke, External infrared reflection absorption spectrometry of monolayer films at the air–water interface, Annu. Rev. Phys. Chem. 46 (1995) 305–334.
[43] Z. Zhang, A.L. Verma, M. Yoneyama, K. Nakashima, K. Iriyama, Y. Ozaki, Molecular orientation and aggregation in Langmuir-Blodgett films of 5-(4-N-octadecylpyridyl)-10,15,20-tri-p-tolylporphyrin studied by ultraviolet-visible and infrared spectroscopies, Langmuir 13 (1997) 4422–4427.
[44] J.M. Vanderkooi, J.L. Dashnau, B. Zelent, Temperature excursion infrared (TEIR) spectroscopy used to study hydrogen bonding between water and biomolecules, Biochim. Biophys. Acta, Prot.Proteomics 1749 (2005) 214–233.